Bending effect on modal interference in a fiber taper and sensitivity enhancement for refractive index measurement

Li-Peng Sun, Jie Li,* Yanzhen Tan, Shuai Gao, Long Jin, and Bai-Ou Guan

Institute of Photonics Technology, Jinan University, Guangzhou 510632, China
tjieli@jnu.edu.cn

Abstract: We demonstrate the bending effect of microfiber on interference fringes in a compact taper-based modal interferometer and sensitivity for refractive index (RI) measurement. For the bend curvature ranging from 0 to 0.283 mm^{-1}, the measured RI sensitivity distinctively increases from 342.5 nm/RIU (refractive-index unit) to 1192.7nm/RIU around RI = 1.333 and from 3847.1 nm/RIU to 11006.0 nm/RIU around RI = 1.430, respectively. Theoretical analysis reveals that such enhancement is determined by the dispersion property of the intermodal index rather than other parameters, such as the variation of the straightforward evanescent field. The magnitude of sensitivity varies as a function of the microfiber bend curvature. Approaching a critical curvature (the intermodal-index dispersion factor approaches zero), the sensitivity is significantly enhanced, exhibiting great potential in RI sensing areas.

OCIS codes: (060.2370) Fiber optics sensors; (260.3160) Interference; (230.3990) Micro-optical devices; (230.1150) All-optical devices.

References and links

1. B. H. Lee and J. Nishii, "Dependence of fringe spacing on the grating separation in a long-period fiber grating pair," Appl. Opt. **38**(16), 3450–3459 (1999).
2. G. Laffont and P. Ferdinand, "Tilted short-period fibre-Bragg-grating-induced coupling to cladding modes for accurate refractometry," Meas. Sci. Technol. **12**(7), 765–770 (2001).
3. B. Li, L. Jiang, S. Wang, L. Zhou, H. Xiao, and H. L. Tsai, "Ultra-abrupt tapered fiber Mach-Zehnder interferometer sensors," Sensors (Basel) **11**(12), 5729–5739 (2011).
4. Z. B. Tian and S. S. Yam, "In-line abrupt taper optical fiber Mach–Zehnder interferometric strain sensor," IEEE Photon. Technol. Lett. **21**(3), 161–163 (2009).
5. K. Q. Kieu and M. Mansuripur, "Biconical fiber taper sensors," IEEE Photon. Technol. Lett. **18**(21), 2239–2241 (2006).
6. T. Wei, X. Lan, and H. Xiao, "Fiber inline core–cladding-mode Mach–Zehnder interferometer fabricated by two-point CO_2 laser irradiations," IEEE Photon. Technol. Lett. **21**(10), 669–671 (2009).
7. J. Yang, L. Jiang, S. Wang, B. Li, M. Wang, H. Xiao, Y. Lu, and H. Tsai, "High sensitivity of taper-based Mach-Zehnder interferometer embedded in a thinned optical fiber for refractive index sensing," Appl. Opt. **50**(28), 5503–5507 (2011).
8. M. Zibaii, O. Frazao, H. Latifi, and P. A. S. Jorge, "Controlling the sensitivity of refractive index measurement using a tapered fiber loop mirror," IEEE Photon. Technol. Lett. **23**(17), 1219–1221 (2011).
9. Z. B. Tian, S. S. Yam, and H. P. Loock, "Refractive index sensor based on an abrupt taper Michelson interferometer in a single-mode fiber," Opt. Lett. **33**(10), 1105–1107 (2008).
10. G. Salceda-Delgado, D. Monzon-Hernandez, A. Martinez-Rios, G. A. Cardenas-Sevilla, and J. Villatoro, "Optical microfiber mode interferometer for temperature-independent refractometric sensing," Opt. Lett. **37**(11), 1974–1976 (2012).
11. C. Zhong, C. Shen, Y. You, J. Chu, X. Zou, X. Dong, Y. Jin, and J. Wang, "Temperature-insensitive optical fiber two-dimensional micrometric displacement sensor based on an in-line Mach–Zehnder interferometer," J. Opt. Soc. Am. B **29**(5), 1136–1140 (2012).
12. H. Y. Choi, M. J. Kim, and B. H. Lee, "All-fiber Mach-Zehnder type interferometers formed in photonic crystal fiber," Opt. Express **15**(9), 5711–5720 (2007), http://www.opticsinfobase.org/oe/abstract.cfm?id=132856.
13. G. Brambilla, "Optical fibre nanowires and microwires: a review," J. Opt. **12**(4), 043001 (2010).
14. H. Xuan, W. Jin, and M. Zhang, "CO_2 laser induced long period gratings in optical microfibers," Opt. Express **17**(24), 21882–21890 (2009).

#196089 - $15.00 USD Received 3 Sep 2013; revised 20 Oct 2013; accepted 23 Oct 2013; published 29 Oct 2013

15. J.-L. Kou, M. Ding, J. Feng, Y.-Q. Lu, F. Xu, and G. Brambilla, "Microfiber-based Bragg gratings for sensing applications: A Review," Sensors (Basel) **12**(12), 8861–8876 (2012).
16. J. Li, L.-P. Sun, S. Gao, Z. Quan, Y.-L. Chang, Y. Ran, L. Jin, and B.-O. Guan, "Ultrasensitive refractive-index sensors based on rectangular silica microfibers," Opt. Lett. **36**(18), 3593–3595 (2011).
17. D. T. Cassidy, D. C. Johnson, and K. O. Hill, "Wavelength-dependent transmission of monomode optical fiber tapers," Appl. Opt. **24**(7), 945–950 (1985).
18. D. Marcuse, "Curvature loss formula for optical fibers," J. Opt. Soc. Am. A **66**(3), 216–220 (1976).
19. M. Koshiba and Y. Tsuji, "Curvillinear hybrid edge/nodal elements with triangular shape for guided-wave problems," J. Lightwave Technol. **18**(5), 737–743 (2000).
20. M. Bass, Handbook of Optics, 3rd ed. (McGraw-Hill, 2009).
21. K. F. Palmer and D. Williams, "Optical properties of water in the near infrared," J. Opt. Soc. Am. **64**(8), 1107–1110 (1974).

1. Introduction

Optical fiber Mach-Zehnder interferometers, which use two separated optical signals to produce interference fringes, have been widely studied in both optical commutation and sensor systems. Recently, modal interferometers that superimpose different fiber modes with dissimilar effective indices in a single fiber device have attracted considerable attention due to their advantages such as compactness, easy implementation, high fringe visibility, and robustness. Various approaches have been proposed to excite/recombine the interferometric modes by the use of long-period grating [1], tilted fiber Bragg grating [2], abrupt fiber taper [3–10], or connection of a standard single-mode fiber to a special fiber such as polarization maintaining fiber [11] or photonic crystal fiber [12]. Difficulty is control over the spectral characteristics after the device fabrication.

Refractive index (RI) sensing becomes one of the most attractive applications for those modal interferometers [3–10] since the modes have different responses to external RI variation. The device performance is mostly governed by the sensitivity, defined as a relative shift in a dip or peak due to a unity change of external RI, and mainly depends on the interaction between the evanescent field and the external RI. To date, much attention has been paid to decrease the microfiber scale in order to increase the sensitivity of RI sensing. The schemes include microfiber resonators [13], gratings [14, 15], loop mirrors [16], and interferometers [3–10]. However, too thin component size is not favorable to maintain the high mechanical property of microfibers in the real-world applications. In this paper we present an alternative method for enhancement of RI sensitivity by bending the microfiber in a single taper-based modal interferometer. Both experimental investigation and theoretical analysis are performed and show good agreement with each other.

2. Bending effect on fringes of a single taper-based modal interferometer

Figure 1(a) illustrates the schematic of our taper-based modal interferometer with a microfiber bend. The structure is obtained by locally heating and stretching a highly Ge-doped fiber (Coractive, UVS-INT, NA = 0.20) with assistance of a flame-brush technique [13]. Similar to the well-established biconical model [13], the fabricated structure comprises a central uniform microfiber that is connected with two transition regions, as shown in Fig. 1(a). The transition has an abrupt change in diameter to break the adiabaticity, so that the coupling could occur between waveguide modes [9]. Unlike the common communication single-mode fibers (such as SMF-28) [9,10], the UVS-INT fiber has a relatively large index contrast between the core and the cladding due to the high Ge doping concentration in the core. The remaining Ge dopant in a tapered fiber is still high to well separate the fundamental and the higher-order modes and to induce the π phase shift easily in the taper. Although more than two modes may be excited, mode beating is mainly between the HE_{11} and HE_{12} modes because they have the similar azimuthal symmetry and the smallest phase mismatch [17].

As shown in Fig. 1(a), the light beam is partially coupled into the HE_{11} and HE_{12} modes at the incident transition and experiences different effective indices in the microfiber. The interference is given by recombination of the modes at the output transition, with the resultant phase difference Φ:

#196089 - $15.00 USD Received 3 Sep 2013; revised 20 Oct 2013; accepted 23 Oct 2013; published 29 Oct 2013

$$\Phi = (2\pi/\lambda)\Delta n \cdot L \tag{1}$$

where $\Delta n = n_{eff1} - n_{eff2}$ represents the intermodal index with n_{eff1} and n_{eff2} the effective indices for the HE_{11} and HE_{12} modes, respectively, L is the interaction length of the modes, and λ is the wavelength. The transmittance is approximately given by $T = \cos^2(\Phi/2)$. The transmission maxima occur at the points when Φ equals an even number of π and the minima occur at the points when Φ equals an odd number of π. The effective indices shown in Eq. (1) can be solved using the wave equation [13], given that the refractive index profile is known. We adopt a local mode model as has been demonstrated in conventional slab waveguides or fibers [18] for the mode analysis at the microfiber bend. When a mode travels over the bend, the local group velocity along the phase fronts of the mode decreases on the inside while increases on the outside of the bend to maintain a constant angular velocity. As shown in Fig. 1(b), the equivalent index profile along the cross section of a bent microfiber is approximately expressed as

$$n' = n\sqrt{1 + 2x\xi} \tag{2}$$

where n is the real index profile in the microfiber bend, x is perpendicular to the microfiber axis, and $\xi = 1/R$ is the bend curvature with R the bend radius as shown in Fig. 1(a). From Eq. (2), the index rises on the outside but drops on the inside of the waveguide bend compared to the original value. Figure 1(c) shows a picture of a fabricated structure.

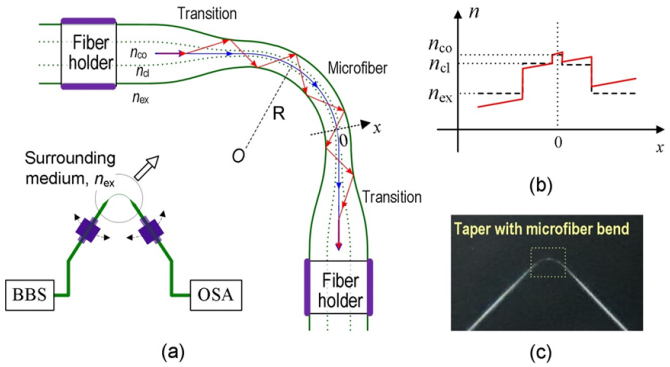

Fig. 1. (a) Schematic of a compact, single taper-based modal interferometer with a microfiber bend. (b) Equivalent refractive index profile in bent microfiber. (c) Picture of a fabricated structure.

Figure 2(a) plots transmission spectra of our taper-based interferometer with ① $\xi = 0$ and ② 0.15mm^{-1}, respectively, by the use of a broadband light source (BBS) and an optical spectrum analyzer (OSA). The taper profile is also provided as an inset of the figure. The total taper length is around 16.9mm and the transition length is around 3.2mm. A strong interference pattern is observed. The typical insertion loss is ~2.0dB and the maximum extinction ratio is higher than 20dB in Fig. 2(a). We fix the two ends of the taper with two fiber holders and bend the microfiber by changing the positions of the holders, as shown in Fig. 1(a). Strictly speaking, when the structure is bent, the bend is made along the whole structure. But because the microfiber has a much smaller size than the untapered fiber, the bend is mainly in the microfiber rather than other areas. During the microfiber bending, the spectral dips blueshift and the spacing of dips becomes large accordingly, as detailed in Fig. 2(b). For example, for the curvature changing from 0 to 0.15 mm^{-1}, the dip wavelength blueshifts from 1510.8nm to 1418.9nm with a range of ~91.9 nm and simultaneously, the dip spacing slightly increases from 44.6nm to 51.9nm around wavelength 1500nm.

The mode characteristics can be calculated by considering a scaled-down UVS-INT fiber model with the help of a full-vector finite element method [19]. This model has a diameter

#196089 - $15.00 USD Received 3 Sep 2013; revised 20 Oct 2013; accepted 23 Oct 2013; published 29 Oct 2013

ratio between the core and the cladding of 6.1μm/125μm, a core-cladding index contrast of 0.0125, a silica fiber diameter of 20μm, and an interaction length of modes with 10.5mm, respectively. Note that although a UVS-INT fiber contains an inner cladding which is used to heighten the photosensitivity of the fiber, it has been ignored in our calculation due to same index to the outer cladding. The material dispersion of the fused silica [20] in the cladding is taken into account. By substituting the effective indices of the modes into Eq. (1), the transmission is calculated and plotted in Figs. 2(a) and 2(b). The calculation shows good agreement with the experimental values. Investigation shows that bending the microfiber increases the intermodal index Δn and thus shifts the wavelength of the interferometer. The variation of wavelength, on the other side, alters the Δn value in Eq. (1) due to the dispersion characteristic of Δn. Normally, Δn becomes large with an increase of wavelength. To understand the behavior of wavelength shift, we take small variations of curvature and wavelength, i.e., $\delta\xi$ and $\delta\lambda$, from Eq. (1) and obtain the phase change $\delta\Phi = (2\pi/\lambda^2)L[\lambda(\partial\Delta n/\partial\xi)\cdot\delta\xi - \Gamma\cdot\delta\lambda]$, where $\Gamma = \Delta n - \lambda\cdot\partial\Delta n/\partial\lambda$ represents the dispersion factor of the intermodal index. Analysis shows $\partial\Delta n/\partial\xi > 0$ and $\Gamma < 0$ within the wavelength region of Fig. 2 and thereby the condition of $\delta\Phi = 0$ and $\delta\xi > 0$ produces $\delta\lambda < 0$. With an increase of curvature, the wavelength should blueshift to obtain a small Δn and to keep the phase Φ fixed, consistent to the observation in Fig. 2. The small discrepancy between the experimental and theoretical results is mainly attributed to the existence of nonuniform bend in the microfiber along the interaction length of modes.

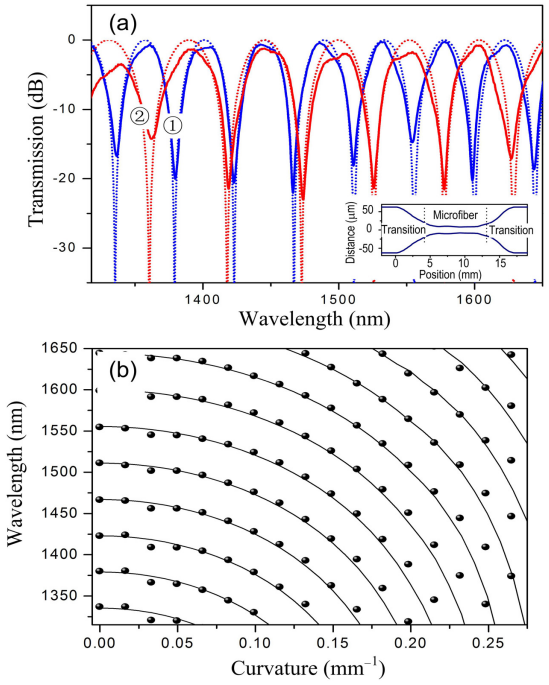

Fig. 2. (a) Measured (solid curves) and modeled (dashed curves) transmission spectra of the interferometer at curvatures: ① $\xi = 0$ mm^{-1} and ② $\xi = 0.15$mm^{-1}, respectively. Inset shows the profile of the fabricated taper-based interferometer. (b) Measured (points) and modeled (solid curves) dip wavelengths in respect of bend curvature.

3. Sensitivity enhancement for refractive index measurement

We measure the response of our taper device to external RI (n_{ex}) by immersing it into an aqueous solution of sucrose, with the solution's index modified by changing the sucrose concentration at room temperature. Figure 3(a) plots the transmission spectra with $n_{ex} = 1.333$

#196089 - $15.00 USD Received 3 Sep 2013; revised 20 Oct 2013; accepted 23 Oct 2013; published 29 Oct 2013

and 1.384, at $\xi = 0$ mm^{-1}, 0.116 mm^{-1}, 0.201 mm^{-1}, 0.283 mm^{-1}, respectively. The microfiber may be broken in a quite severe bend condition in practice. The larger curvature produces the wider dip spacing similar to Fig. 2. With the increasing of external RI from 1.333 to 1.384, the measured wavelengths redshift for around 29.5nm, 34.5nm, 46.4nm, and 68.3nm, respectively, at the dips of *A*~*D* as shown in Fig. 3(a). The larger curvature corresponds to a bigger wavelength shift. Figure 3(b) details the dip-wavelength shifts as functions of external RI for the different curvatures. The measured sensitivities are S = 342.5 nm/RIU (refractive-index unit), 483.6 nm/RIU, 704.0 nm/RIU, 1192.7nm/RIU, respectively, around n_{ex} = 1.333 and S = 3847.1 nm/RIU, 4880.1 nm/RIU, 6325.0 nm/RIU, 11006.0 nm/RIU, respectively, around n_{ex} = 1.430, for the dips *A*~*D* near a wavelength of 1350nm. It is clear that for the curvature increasing from 0 to 0.283 mm^{-1}, the sensitivity is enhanced by 3.48 times around

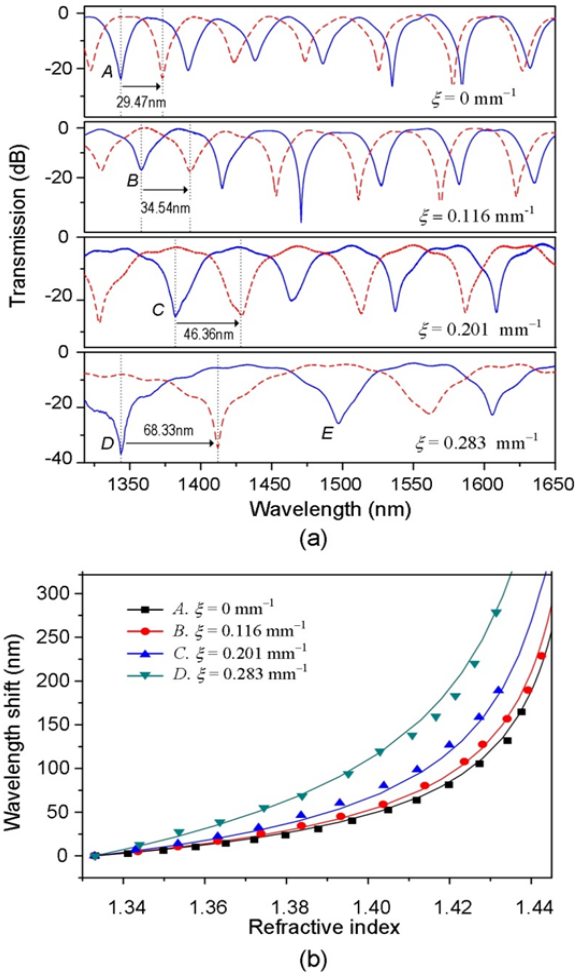

Fig. 3. (a) Transmission spectra of an interferometer with different curvatures immersed in solution with indices of 1.333 (solid curves) and 1.384 (dashed curves), respectively. (b) Measured (points) and modeled (curves) dip wavelength shifts as functions of external RI at different curvatures.

n_{ex} = 1.333 and 2.86 times around n_{ex} = 1.430, respectively. Such enhanced sensitivities are the highest among the fiber modal interferometers as reported to date [3–10]. Simultaneously, we can measure sensitivity of around 1046.0nm/RIU at n_{ex} = 1.333 at dip *E* near a wavelength of 1500nm, as shown in Fig. 3(a). Comparison shows the sensitivity around 1500nm is

#196089 - $15.00 USD Received 3 Sep 2013; revised 20 Oct 2013; accepted 23 Oct 2013; published 29 Oct 2013

smaller than that around 1350nm because the former corresponds to a larger intermodal-index dispersion factor as discussed later. Small fluctuation of fringes as observed in Fig. 3(a) is from the disturbance of other unwanted modes that are excited by the fiber transition and participate in the interference. This effect can be diminished through optimization of the fiber taper during fabrication. Considering a 10 pm resolution of OSA, the detectable minimum RI change is 8.38×10^{-6} RIU around $n_{ex} = 1.333$ and 9.09×10^{-7} RIU around $n_{ex} = 1.430$, respectively, at $\xi = 0.283$ mm^{-1} as shown in Fig. 3. We also investigate the temperature dependency by placing the interferometer into a resistance furnace in air. We record the dip wavelengths for the temperature varying from 30 °C to 90 °C with a step of 10°C and obtain a coefficient of –0.062nm/°C around 1450nm. This temperature dependency may be attributed to the thermal expansion and thermo-optic effects in the core and the cladding of the fiber taper. It is found that bending the microfiber can hardly change the temperature dependency since the mode energies are mainly confined in the silica fiber. The environmental temperature should be kept stable to achieve high accuracy of RI measurement.

A variation of external RI can produce different changes to the dissimilar mode indices, leading to a modification of the intermodal index. To further understand the RI sensitivity, the spectral responsivity on external RI can be achieved by taking a small variation of n_{ex} from Eq. (1) for Φ to be considered unchanged. After several mathematical treatments, we obtain

$$S = \frac{d\lambda}{dn_{ex}} = \frac{\lambda}{\Gamma}\frac{\partial \Delta n}{\partial n_{ex}} \tag{3}$$

From Eq. (3), the determinative parameters of S are the wavelength λ, the RI-induced variation of intermodal index $\partial\Delta n/\partial n_{ex}$, and the dispersion factor Γ. An increase of n_{ex} can normally generate a larger index increment for the HE_{12} mode than that for the HE_{11} mode, producing $\partial\Delta n/\partial n_{ex}<0$. Simultaneously, we have $\Gamma < 0$ since the group velocity of the HE_{11} mode is larger than the HE_{12} mode within the wavelength region shown in Fig. 3. Thereby a positive S is enabled, corresponding to a redshift of wavelength with an increase of external RI, as demonstrated in Fig. 3. According to Eq. (3), an extremely high sensitivity is achieved in case of $\Gamma \sim 0$. The effect of Γ on the RI sensitivity is similar to that of the group birefringence in a polarization interferometer [16]. However the polarization interferometer is based on the use of a highly-birefringent microfiber. Generally, the fiber size should be thin sufficiently to produce a large phase birefringence for the RI measurement [16]. The present structure, however, allows interference of the modes with different mode orders, which can exhibit the advantages of simplicity, robustness, and ease of fabrication. Moreover, bending the microfiber can alter the dispersion factor Γ and thus change the RI sensitivity from Eq. (3). We conduct a numerical simulation by taking into account the material dispersion of aqueous liquid [21] using a full-vector finite element method [19]. As shown in Fig. 3(b), the calculated results can agree with the experimental values very well. From Eq. (3), the calculated sensitivities are S ' = 415.38 nm/RIU, 454.84 nm/RIU, 573.97 nm/RIU, 1035.80 nm/RIU, respectively, around $n_{ex} = 1.333$ and S ' = 4797.54 nm/RIU, 5389.38 nm/RIU, 6944.23 nm/RIU, 9940.13nm/RIU, respectively, around $n_{ex} = 1.430$, at dips of A~D, respectively. At dip E, the sensitivity is S ' = 813.28 nm/RIU around $n_{ex} = 1.333$.

To further understand the effect of bending microfiber on the magnitude of sensitivity, Fig. 4(a) models the sensitivity as a function of the bend curvature at a wavelength of 1350 nm. The experimental points are marked as comparison. Other than the redshift at $\xi < 0.365$ mm^{-1}, the increasing of external RI can induce a blueshift of wavelength at $\xi > 0.365$ mm^{-1}. Close to the critical curvature of $\xi = 0.365$ mm^{-1} (Γ approaches zero), the sensitivity is enhanced significantly. Moreover, Fig. 4(b) plots the calculated critical curvature as a function of the microfiber diameter at wavelength 1350nm and the wavelength at microfiber diameter 20μm, respectively. A larger microfiber diameter or a shorter wavelength is readier to produce the smaller critical curvature, of which the study is useful for design and optimization of the device in real-world applications. Note that the sensitivity shown in Eq.

#196089 - $15.00 USD Received 3 Sep 2013; revised 20 Oct 2013; accepted 23 Oct 2013; published 29 Oct 2013

(2) is achieved at a specific wavelength point. Considering a spectral width in a dip, the infinite sensitivity cannot be achieved in practice.

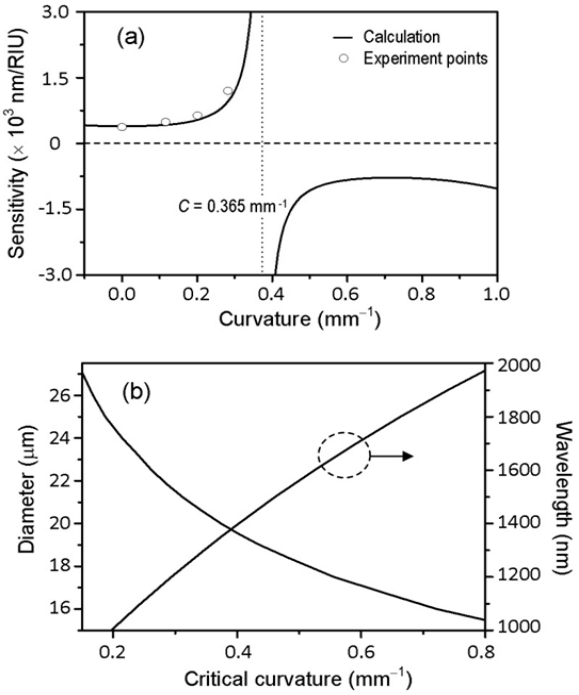

Fig. 4. (a) Modeled sensitivity as a function of bend curvature at wavelength 1350nm. The experimental points are also marked. (b) Dependence of the critical curvature on the fiber diameter at wavelength 1350nm and the wavelength at fiber diameter 20μm, respectively.

4. Conclusion

In conclusion, we study the bending effect of microfiber on the interference fringes and sensitivity for RI measurement in a compact taper-based modal interferometer. Bending microfiber can induce an obvious variation of the transmission spectrum of the device. For the curvature ranging from 0 to 0.283 mm^{-1}, the sensitivity increases dramatically from 342.5 nm/RIU to 1192.7nm/RIU around RI = 1.333 and from 3847.1 nm/RIU to 11006.0 nm/RIU around RI = 1.430, respectively. Such high sensitivity is mainly governed by the dispersion property of the intermodal index rather than other parameters, e.g., the variation in the evanescent field. The magnitude of sensitivity varies as a function of the bend curvature. Close to the critical curvature (the intermodal-index dispersion factor approaches zero), the sensitivity will be enhanced significantly. We provide both the detailed experimental and theoretical investigations, which show good agreement with each other. The dependence of the critical curvature on the fiber diameter and the wavelength is also discussed. The research results are important and valuable for future applications of the device.

Acknowledgments

This work is supported by the National Natural Science Foundation of China (61225023, 61177074, 11004085, and 11104117), the Project of Science and Technology New Star of Zhujiang in Guangzhou city (2012J2200062), the Research Fund for the Doctoral Program of Higher Education of China (20114401110006), and the Guangdong Natural Science Foundation (S2013030013302).